From Flood Risk to Caloric Loss: Compound Flood Impacts on Agriculture in Madagascar

Celina Thomé
Heidelberg University, Germany
celinathome@gmx.de

Anne Schauß
Heidelberg Institute for Geoinformation Technology (HeiGIT), Germany
anne.schauss@heigit.org

Marcel Maurer
Heidelberg Institute for Geoinformation Technology (HeiGIT), Germany
marcel.maurer@heigit.org

apl. Prof. Dr. Sven Lautenbach
Heidelberg University, Germany
sven.lautenbach@uni-heidelberg.de

Prof. Dr. Alexander Zipf
Heidelberg University, Germany
zipf@uni-heidelberg.de

Dr. Yulia Grinblat*
Heidelberg Institute for Geoinformation Technology (HeiGIT), Germany
yulia.grinblat@heigit.org

ABSTRACT

Flood hazards increasingly threaten food production in Madagascar, yet spatially explicit assessments that translate flood exposure into nutritionally meaningful impacts remain limited. This study develops a spatially explicit framework that combines nationwide crop type mapping, compound flood hazard scenarios, and depth-dependent crop damage functions to estimate flood-induced caloric losses under baseline conditions (2020) and future climate pathways (2030, 2050, and 2080; SSP1, SSP2, SSP3, and SSP5). A custom crop classification model achieved 72% overall accuracy and enabled mapping of key staple crop groups across Madagascar. Potential caloric production was then estimated and combined with compound flood depth maps to derive crop-specific relative losses, district-level spatial impact patterns, and national absolute caloric loss trajectories. Under the 2020 baseline flood scenario, estimated caloric losses translate to people not being fed, equivalent to the annual minimum dietary energy requirement of about 3.3 million people in a 1-in-5-year event and more than 9 million people in a 1-in-100-year event, with impacts increasing for rarer floods and intensifying under high-emission futures. By shifting the proxy from flooded area to human-centred indicators (calories and people-equivalents), the framework provides decision-relevant evidence for preparedness planning, anticipatory action, and humanitarian prioritisation.

Keywords

Compound Flooding, Agricultural Vulnerability, Caloric Loss Assessment, Food Security, Impact-Based Forecasting

INTRODUCTION

Madagascar is highly exposed to climate-related hazards, particularly tropical cyclones and flooding, which repeatedly disrupt livelihoods, infrastructure, and agricultural production (Kruger, 2016; World Bank Group, 2024). Because staple crop production remains central to basic food-energy supply, flood impacts on agriculture can rapidly reduce caloric availability in vulnerable regions (Cassidy et al., 2013; Rigden et al., 2022; Thompson et al., 2012). At the same time, flooding in Madagascar is rarely driven by a single mechanism. Instead, intense rainfall, riverine overflow, and coastal storm surge frequently interact, producing complex multi-hazard events whose consequences are difficult to assess with conventional single-hazard approaches (Khan et al., 2025; Wing et al., 2024).

*corresponding author

For crisis management, the challenge is not only to detect hazards, but to translate hazard information into forms that are meaningful for decision-making. Existing assessments often report flooded area, exposed cropland, or generalized production losses. While such indicators are useful, they provide limited guidance on where flood impacts are most likely to reduce caloric availability, which districts may require prioritised intervention, and how limited preparedness or response resources should be allocated (Budhathoki et al., 2024; Pacetti et al., 2017). In this sense, compound flooding poses not only a hazard-modelling challenge, but also an information-systems challenge: heterogeneous geospatial, agricultural, and hazard data must be integrated, processed, and transformed into decision-relevant impact indicators.

This information gap is especially pronounced in data-scarce contexts such as Madagascar. Existing cropland products provide information on cropland extent, but generally do not distinguish between crop types (Brown et al., 2022; Lou et al., 2025; Teluguntla et al., 2015). National agricultural statistics report production volumes, yet lack the spatial detail required to relate hazard exposure to localised losses in caloric availability (European Commission, 2025; Food and Agriculture Organization of the United Nations [FAO], 2025; Foreign Agricultural Service, 2025; Global Yield Gap Atlas, 2025). As a result, crisis actors often have access either to hazard information without clear impact interpretation, or to production statistics without spatial exposure context. What remains limited is an operational framework that links hazard, exposure, and impact in a way that supports anticipatory action and crisis response.

Only a limited number of studies have translated agricultural production or losses into caloric terms or estimated the number of people supported by available production (Cassidy et al., 2013; Gonzales-Valero, 2018; Pacetti et al., 2017). At the global scale, Cassidy et al. (2013) examine calorie availability under alternative crop allocation scenarios, highlighting food-system efficiency rather than climate hazards. At the regional scale, Gonzales-Valero (2018) estimate caloric availability under different climatic conditions in Peru, yet rely on aggregated statistics without spatial exposure modelling. Event-based analyses by Pacetti et al. (2017) demonstrate how flood-induced crop losses can be translated into caloric loss, but focus on individual historical events and depend on detailed site-specific data. Together, these studies highlight the value of nutritionally meaningful indicators while also showing that spatially explicit, scenario-based approaches for compound flood impacts remain limited.

Recent advances in GeoAI and flood modelling create new opportunities to address this limitation. Multi-sensor time series can support crop classification at large scales, and combining optical and radar data has been shown to improve classification accuracy (Orynbaikyzy et al., 2019). However, national-scale crop type products remain scarce for Madagascar. Existing studies either focus on prediction of production without spatial crop maps (Rigden et al., 2022) or are limited to regional case studies (Lelong & Herimandimby, 2022; Stéphane et al., 2020). More broadly, the availability of representative training data remains a persistent challenge in data-scarce regions (Eisfelder et al., 2024). At the same time, high-resolution flood models provide scenario-based estimates of floods under present and future conditions (Wing et al., 2024). Together, these developments enable the integration of heterogeneous environmental and agricultural data into decision-support information that can support anticipatory action, preparedness planning, and humanitarian prioritisation under compound flood risk.

Against this background, this study develops a spatially explicit, impact-oriented decision-support framework for assessing compound flood impacts on agricultural production in Madagascar. The framework integrates crop type mapping, compound flood scenarios, and crop-specific damage assumptions in order to derive indicators of reduced caloric availability. More specifically, the analysis first establishes a baseline map of cultivated crop types, then estimates potential caloric production under non-flooded conditions, and finally quantifies how flood exposure translates into caloric loss through depth-dependent yield damage. The resulting indicators are expressed in terms of caloric losses and people-equivalent shortfalls and are aggregated to administrative units to support spatial comparison and prioritisation.

The contribution of the study lies not only in estimating flood-induced caloric losses, but in structuring those estimates as decision-support information for compound flood response. By translating multi-hazard flood exposure into actionable indicators of impact on caloric availability, the framework contributes to crisis information systems research and supports anticipatory action, preparedness planning, and humanitarian prioritisation under climate uncertainty.

METHODOLOGY

Overview of the Workflow

The methodological workflow used to estimate flood-induced caloric losses under compound flood scenarios is shown in Figure 1. The workflow combines flood hazard information, crop type classification, crop-specific caloric values, and depth-dependent damage assumptions in order to derive decision-relevant impact indicators.

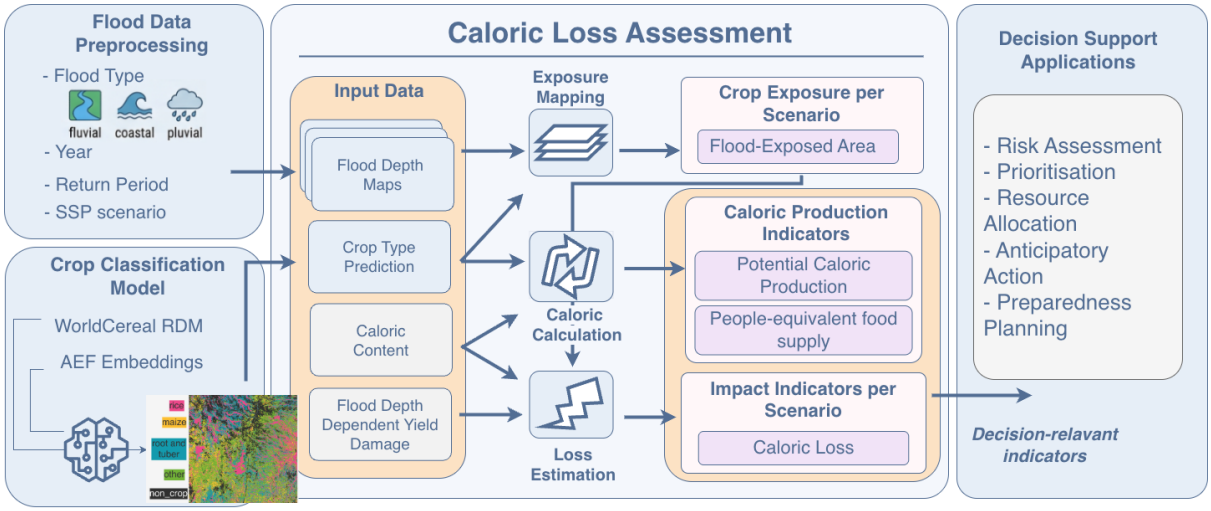

Figure 1. Caloric loss assessment workflow and decision-support indicators.

The analysis consists of four main steps. First, a custom crop type classification model was used to generate a spatially explicit baseline map of crop and non-crop classes across Madagascar. This map represents the estimated distribution of key staple crop groups and does not predict future planting decisions. Second, the mapped crop areas were converted into potential caloric production using crop-specific caloric values per hectare, yielding baseline indicators of caloric production and people-equivalent food supply. Third, compound flood depth maps were combined with the crop map to derive flood-exposed crop areas for each scenario, defined by return period, time horizon, and SSP pathway. Fourth, flood depth was translated into crop-specific yield damage and resulting caloric loss using depth-dependent loss functions. The resulting impact indicators were then aggregated to administrative units to compare food-production impacts across districts and scenarios.

From an information systems perspective, the workflow can be understood as a data-to-decision pipeline. It integrates heterogeneous geospatial data from multiple sources on hazards and land use, applies analytical models to derive impact estimates, and produces aggregated indicators at the administrative level. By translating physical hazard exposure into food-security-relevant metrics, the framework reduces analytical complexity and supports decision-makers in identifying high-impact areas and prioritizing interventions.

Input Data

Flood Hazard Data

The flood data used in this study are derived from the Fathom Global Flood Model (Sampson et al., 2015; Wing et al., 2024) , a high-resolution global dataset with a spatial resolution of 30 m (Fathom, 2024). The dataset includes hazard layers for three distinct flood perils—fluvial, pluvial, and coastal flooding—across ten Return Periods, which represent flood events of different recurrence likelihoods and severity. In addition to present-day conditions, it provides projections for future time horizons (2030, 2050, and 2080), enabling assessment of how flood exposure may evolve under changing climatic conditions.

Future hazard projections are available for multiple Shared Socioeconomic Pathways (SSPs), here represented by SSP1, SSP2, SSP3, and SSP5, which capture alternative climate and development futures ranging from lower- to higher-emission trajectories. This allows comparison of potential flood impacts across both time horizons and climate pathways.

The dataset further distinguishes between defended and undefended conditions. Defended scenarios apply generalized protection standards calibrated to national income levels, reflecting a lower assumed likelihood of flooding in countries with greater defence capacity. However, these scenarios do not incorporate information on the location, type, or performance of specific physical flood protection structures (Wing et al., 2024). In this study, only defended scenarios were used, as they provide a more realistic approximation of present-day flood exposure than fully undefended conditions, while still not representing the exact location and performance of local protection infrastructure.

Table 1. Reference data summary by crop group.

Crop group	Reference locations (n)	Share (%)	Total observations	Avg obs/ location	Observation period
Rice	761	10.5	13,441	17.7	2016 to 2019
Maize	297	4.1	5,256	17.7	2016 to 2019
Root and tuber	299	4.1	5,453	18.2	2016 to 2019
Other crops	2,331	32.2	43,493	18.7	2016 to 2021
Non-crop areas	3,557	49.1	70,546	19.8	2016 to 2022
Total	**7,245**	**100.0**	**138,189**	**19.1**	**2016 to 2022**

Reference Data for Crop Classification

WorldCereal is a global crop mapping system developed under the ESA WorldCereal programme, providing cropland, crop type and irrigation products at 10 m resolution (Van Tricht et al., 2023). Accurate, spatially explicit crop information is essential for agricultural monitoring, policy-making as well as food and water security assessments. In addition to its global default crop-mapping model for 2021, WorldCereal supports custom training for specific regions using user-provided crop labels and multi-sensor Earth Observation (EO) time series, while more recent work has explored the integration of advanced AI foundation models such as Presto into the WorldCereal workflow (Butsko et al., 2025). However, this custom training is recommended only for relatively small areas due to computational and credit constraints. In the present study, the WorldCereal reference data were therefore used exclusively as training labels, whereas the crop type classification was implemented through a separately developed custom model for nationwide mapping in Madagascar.

To leverage high-quality reference data without these limitations, the WorldCereal Reference Data Module (RDM) for Madagascar was used. The RDM consolidates datasets from multiple providers under unified metadata and applies both automated quality checks and manual curation to provide a consistent and reliable training dataset (WorldCereal, 2026).

In line with Madagascar's four main staple crops, which together account for approximately 75 % of the daily caloric intake, the model was designed to distinguish between rice, maize, cassava, sweet potato and potato. However, the number of available reference samples for potato, sweet potato and cassava was insufficient for stable per-class learning. These categories were therefore combined into a single class, root and tuber crops.

Overall, the RDM contains 7,245 reference locations for Madagascar collected between 2016 and 2022, with each location having between 16 and 40 observations (Table 1). In total, this corresponds to 138,189 temporal observations, with an average of 19.1 observations per location. These data formed the foundation for developing a custom crop type classification model tailored to the study area.

AlphaEarth Foundation embeddings

AlphaEarth Foundation (AEF) embeddings were used as the primary remote sensing data. AEF is a geospatial AI foundation model that fuses multi-sensor EO time series into compact, analysis-ready embedding vectors that capture spatial structure and temporal dynamics and are robust to missing or noisy observations (Brown et al., 2025). In this study, the 2024 annual embedding layer from the Google Earth Engine (GEE) *AEF Embedding* dataset was used, provided as a global 10 m image with 64 embedding dimensions per pixel. The embeddings were retrieved for the full extent of Madagascar in GEE and used as input features for the crop type classification model.

Analytical Workflow

Custom Crop Type Classification Model

A custom crop type classifier was implemented using CatBoost (Prokhorenkova et al., 2018), a tree-based gradient boosting algorithm well suited to tabular data with heterogeneous feature spaces and class imbalance. Using the WorldCereal RDM reference data as training labels enabled the model to integrate spectral reflectance bands derived from remote sensing imagery with AEF embeddings from 2024 as input features (Brown et al., 2025). The classification target, *crop_type*, comprised five classes: maize, rice, root and tuber crops, other crops, and non-crop areas.

The dataset was split into training (70 %), validation (15 %) and test (15 %) subsets using stratified sampling to preserve class proportions, ensuring that all classes were represented across splits and mitigating the effects of class

imbalance. To address class imbalance, class weights were specified inversely proportional to class frequency in the training dataset. To prioritize the prediction's accuracy of key staple crops, the class weights of maize and rice were increased by a factor of 3 and 1.5, respectively, whereas the rest classes retained the standard inverse-frequency weighting.

The CatBoost classifier was configured with a one-vs-all multi-class loss (*MultiClassOneVsAll*) and evaluated using the total F1 score. Key hyperparameters included a learning rate of 0.03, maximum tree depth of 8, L2 regularization of 6.0, feature subsampling (RSM) of 0.8, bagging temperature of 0.5 and random strength of 1.0. Early stopping based on the validation set was applied to prevent overfitting. Model selection was based on validation performance, and the selected model was subsequently applied to the held-out test split for final evaluation.

Potential Caloric Production Estimation

Potential caloric production was estimated by combining the spatial distribution of cultivated crop types with crop-specific caloric values per hectare. This step provides a baseline measure of potential caloric availability under non-flooded conditions. For each crop class, mapped crop areas were multiplied by the corresponding average caloric content per hectare to derive spatially explicit estimates of annual caloric production (Table 2). Areas classified as "other crops" were assigned an average caloric content of ~6,500,000 kcal/ha (Sands, 2020).

The resulting baseline represents the theoretical caloric contribution of cultivated areas and serves as the reference against which flood-induced losses were calculated. Potential caloric availability was estimated separately for each crop class and subsequently aggregated to district level to support spatial comparison of food-production capacity across Madagascar.

Flood Exposure Mapping

The flood hazard data comprise four time horizons (2020, 2030, 2050, and 2080), multiple SSP-based climate pathways, and three flood perils: coastal, fluvial, and pluvial flooding. To represent compound flooding, these hazard layers were merged into a single flood-depth surface by retaining the maximum pixel value across peril types for each scenario. This approach reflects the interacting nature of flood processes in Madagascar and follows findings by Khan et al. (2025), who show that cyclone-induced flooding is inherently compound and that neglecting interacting drivers can substantially underestimate total risk.

Although the underlying hazard dataset contains a much larger scenario space, the analysis presented here focuses on four return periods (1-in-5, 1-in-10, 1-in-50, and 1-in-100 years) under baseline conditions and future SSP pathways. This selection captures a range of event severities, from relatively frequent shocks relevant to anticipatory action and preparedness planning to rarer, high-magnitude events that serve as stress tests for longer-term agricultural adaptation and disaster risk reduction. Flood-exposed crop areas were derived separately for each combination of return period, time horizon, and SSP pathway.

Crop Damage and Caloric Loss Estimation

Flood-induced caloric loss was estimated by combining the previously derived potential caloric production with spatially explicit flood-depth data, crop-specific yield-loss functions, and crop-specific caloric values. Depth-dependent yield-loss factors were applied to the baseline caloric availability in order to estimate flood-induced caloric losses.

As large-scale flood hazard models provide scenario-based approximations rather than exact event-specific predictions, flood depth was used as a proxy for flood severity. Rule-based thresholds were derived from literature linking flood depth to crop losses (Adarsha et al., 2019; Alves et al., 2024; Budhathoki et al., 2024; Molinari et al., 2019; Neubert et al., 2020; Park et al., 2022), under the assumption that deeper inundation generally corresponds to longer-lasting or more destructive flood conditions. Crop-specific damage thresholds and yield-loss ranges were then translated into discrete depth-dependent loss functions (Table 2). Rice was assumed to be relatively flood tolerant, with damage increasing above 0.5 m flood depth (Budhathoki et al., 2024; Park et al., 2022). Maize was treated as highly sensitive to flooding, particularly during early growth and flowering stages (Adarsha et al., 2019; Molinari et al., 2019). Root and tuber crops were assumed to be vulnerable to excess soil moisture and prolonged waterlogging (Alves et al., 2024; Roberts & Russo, 1991). Other crops were assigned an intermediate sensitivity; where crop-specific depth-damage relationships were unavailable, the conservative loss function for root and tuber crops was applied. Where stage- or duration-specific information was available, mean loss values were used to approximate expected damage under unknown timing conditions. This simplification introduces uncertainty, as flood depth alone cannot fully capture stage-specific or duration-dependent crop responses. Consequently, the resulting damage estimates should be interpreted as approximate rather than exact.

Table 2. Crop-specific caloric values and flood-depth-dependent yield loss assumptions by crop and growth stage.

Crop	Caloric content (kcal/ha)	Stage	<50 cm	50–100 cm	101–125 cm	>125 cm
Maize	20,831,000	Initial	100%			
		Growing / Flowering	0–70%			100%
		Maturing	0%			0–100%
		Stage avg.	45%			83.3%
Rice	11,542,900	–	0–10%	10–70%	40–100%	
Root and tuber	10,775,400	–	36–53%			
Other crops	~6,500,000 (avg.)	–	36–53%			

Flood exposure was estimated at the pixel level by overlaying crop-type and flood-depth layers across all scenarios and years. Flooded crop areas were then translated into caloric losses by combining crop-specific caloric values (Table 2) with depth-dependent yield-damage factors. For each crop, flood scenario, and depth category, caloric loss was calculated as:

$$\text{Caloric Loss} = A_{\text{flooded}} \cdot D_{\text{yield}} \cdot C_{\text{ha}} \quad (1)$$

where A_{flooded} denotes the flooded area in ha, D_{yield} is the depth-dependent yield damage factor and C_{ha} represents the average caloric content per ha . The estimated outcomes were aggregated to district level to derive total cultivated area, flooded crop area, and the proportion of inundated cropland for each crop class.

RESULTS

Crop Mapping and Potential Caloric Production

Spatially explicit crop type information was generated using a custom classification model trained on multi-source remote sensing data. On the independent test split, the model achieved an overall accuracy of 72% and a macro F1-score of 0.59 (Table 3). The difference between these metrics reflects the imbalanced class distribution in the reference data: strong performance on dominant classes, particularly non-crop areas (F1-score 0.91), increases overall accuracy, whereas the lower macro F1-score indicates more uneven performance across the minority crop classes. Among the staple crop groups relevant for food availability, rice achieved the strongest classification performance (F1-score 0.73), while the heterogeneous *other crops* class showed moderate performance (F1-score 0.55). Maize and root and tuber crops exhibited lower F1-scores (0.38 and 0.40, respectively), indicating weaker class separation. However, both classes showed comparatively high recall, suggesting that the model captured most cultivated areas while also introducing false positives. For downstream production and exposure analyses, this recall-oriented performance is particularly important, as omitted crop areas would lead to systematic underestimation of potential production and flood impacts.

Table 3. Classification performance of the crop type model by class.

Class	Precision	Recall	F1-score	Samples
Rice	0.6715	0.8070	0.7331	114
Maize	0.2537	0.7556	0.3799	45
Root and tuber	0.2967	0.6000	0.3971	45
Other crops	0.7576	0.4286	0.5474	350
Non crops	0.9159	0.9052	0.9105	517
Overall Accuracy			0.7199	1071
Macro F1-score	0.5791	0.6993	0.5936	1071

To assess plausibility at the national scale, the predicted crop areas were compared with available statistics and reference datasets (Table 4). Estimated areas for the major staple crops generally fall within the broad range reported by FAO (FAO, 2025), GYGA (Global Yield Gap Atlas, 2025), FAS (Foreign Agricultural Service, 2025), and EC ASAP (European Commission, 2025), although discrepancies are expected given differences in reporting methods, aggregation levels, crop definitions, and temporal coverage. Rice area was lower than the FAO estimate but remained consistent with other reference sources, while maize and root and tuber crops tended to be underestimated relative to the reported crop yield. The *other crops* category captures cultivated areas that are not explicitly represented in crop-specific reference statistics. At the level of total crop extent, the baseline estimate also differs substantially from the cropland products Dynamic World (Brown et al., 2022) and AFCD (Lou et al., 2025), which report

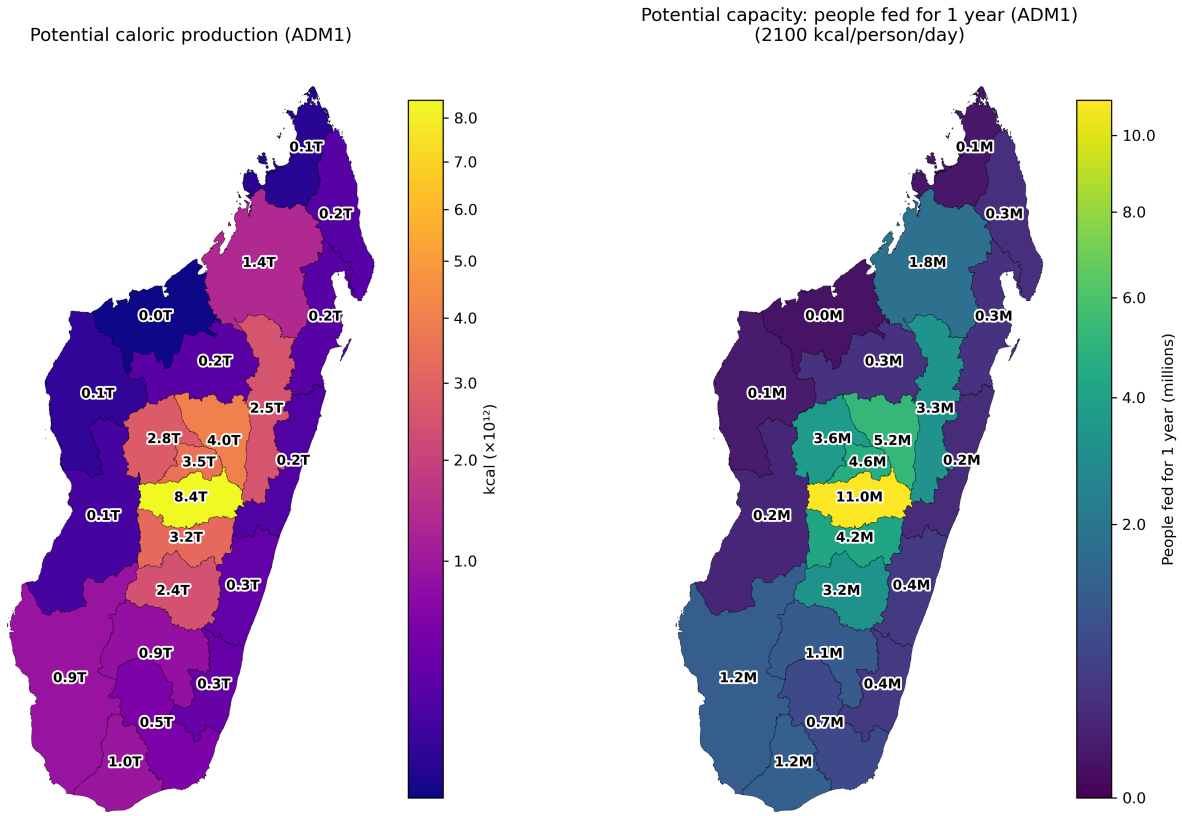

Figure 2. Potential caloric production at ADM1 level (left) and corresponding annual people-fed equivalents based on a minimum requirement of 2,100 kcal per person per day (right).

4,556,816 ha and 1,442,836 ha, respectively. These comparisons should therefore be interpreted as plausibility checks rather than direct validation.

Using the mapped crop areas, potential caloric production was estimated by combining spatial crop distributions with crop-specific caloric values. Figure 2 shows the spatial distribution of total annual caloric production at the district level (left) and the equivalent number of people who could be fed annually (right), assuming 2,100 kcal per person per day as a standard humanitarian planning benchmark (United Nations High Commissioner for Refugees & World Food Programme, 2024; World Food Programme, 2025). Potential caloric production is highly uneven across regions, with major agricultural zones generating large caloric surpluses while other areas remain closer to subsistence levels. These baseline estimates provide the reference against which flood-induced losses are assessed in the following sections.

Table 4. National crop area estimates (ha) from the baseline crop map and reference sources, including total cropland estimates from Dynamic World and AFCD.

Crop type	Baseline	FAO	GYGA	FAS	EC ASAP	Dynamic World	AFCD
Rice	956,733	2,070,335	861,626	1,600,000	1,149,251	–	–
Maize	505,690	148,114	189,640	–	238,629	–	–
Root and tuber	293,771	475,186	464,734	–	520,313	–	–
Other crops	1,652,651	–	–	–	–	–	–
Total crop area	**3,408,845**	–	–	–	–	**4,556,816**	**1,442,836**

Caloric Loss Under Compound Flood Scenarios

Flood impacts on crop production are presented at three complementary levels. First, crop-specific relative caloric losses under selected 2020 baseline return-period scenarios are used to compare the proportional severity of impacts across crop groups. Second, district-level spatial patterns of caloric loss are shown for baseline and future

Table 5. Crop-specific potential caloric production and relative caloric loss under 2020 baseline return-period scenarios.

Crop	Potential calories	Relative caloric loss (%) by return period			
		1-in-5	1-in-10	1-in-50	1-in-100
Rice	10.40×10^{12} kcal	1.5–9.6 %	3.3–16.4 %	8.0–30.5 %	10.1–36.2 %
Maize	9.90×10^{12} kcal	3.2 %	4.6 %	6.6 %	7.7 %
Root and tuber	3.00×10^{12} kcal	1.9–2.8 %	2.7–4.0 %	3.7–5.4 %	4.2–6.2 %
Other crops	10.10×10^{12} kcal	7.5–11.0 %	10.6–15.7 %	14.7–21.6 %	16.3–24.0 %
Total	$\mathbf{33.40 \times 10^{12}}$ kcal	**3.9–7.5 %**	**5.9–11.6 %**	**9.2–18.5 %**	**10.7–21.4 %**

projections in order to identify areas most affected by flood-induced caloric loss. Third, total absolute caloric losses at the national level are reported for 2020, 2030, 2050, and 2080 under SSP1, SSP2, SSP3, and SSP5, enabling comparison across return periods, years, and climate pathways.

Flood exposure varies across crop types (Table 5), with rice generally experiencing the largest impacts because of its concentration in low-lying and flood-prone areas. Across the 2020 baseline scenarios, total relative caloric loss increases from 3.9–7.5 % in the 1-in-5-year event to 10.7–21.4 % in the 1-in-100-year event. Among crop groups, rice shows the highest relative losses under severe flooding, reaching up to 36.2 %, while other crops also experience substantial losses of up to 24.0 %. By contrast, maize and root and tuber crops remain below 10 % and 6.2 %, respectively, even in the 1-in-100-year scenario. These results indicate that flooded area alone does not fully capture impacts on food availability, which also depend on crop productivity and caloric value. The following analyses therefore focus on caloric loss as a more informative indicator of food system impacts.

District-level spatial patterns of caloric loss indicate that the greatest absolute losses occur in the country's main production zones, meaning that floods disproportionately affect regions that underpin national food supply (Figure 3). Absolute caloric losses are greatest in Madagascar's main production districts, particularly in the central highlands around Antananarivo, where baseline caloric production is highest (Figure 2). For example, the central production belt includes districts with potential annual caloric output exceeding 8.4×10^{12} kcal, so even moderate relative losses translate into very large absolute losses. At the same time, several districts along the eastern coast show some of the highest relative losses, in some cases approaching 40–50 % under the more severe return-period scenarios. This indicates that flood impacts are proportionally most severe in these highly exposed coastal districts, despite their lower baseline production.

The national-level scenario analysis complements this crop- and district-specific view by showing total absolute caloric losses across return periods, years, and SSP pathways (Figure 4). All SSP trajectories are anchored to the same 2020 baseline value, so divergence between pathways is shown only for future projections. Under baseline conditions (2020), the 1-in-5-year event results in losses of approximately 2.50×10^{12} kcal, equivalent to the annual minimum dietary energy requirements of about 3.3 million people, while the most severe baseline compound flood (1-in-100-year event) results in losses of approximately 7.13×10^{12} kcal, equivalent to more than 9 million people. Across all return periods, losses increase over time, with differences between climate pathways remaining limited in the near term but becoming more pronounced toward mid- and late century. By 2080, the largest impacts occur under high-emission scenarios, reaching up to 7.57×10^{12} kcal in the SSP5 1-in-100-year event. This corresponds to the annual minimum dietary energy requirements of nearly 9.9 million people and to about 29 % of total potential caloric production.

DISCUSSION

Crop Type Predictions

The crop type classification model based on AEF embeddings performed robustly for the main staple crops, particularly rice, which is captured with high recall and moderate precision. High recall ensures that a large proportion of rice and maize areas are correctly identified, which is critical for subsequent flood exposure and caloric loss analyses. Lower precision for maize and root and tuber crops indicates that some areas may be misclassified, potentially leading to overestimation of exposed areas at the pixel scale. These limitations presumably largely stem from class imbalance in the reference data, spectral similarity among crop types and limited training samples for underrepresented classes. The absence of independent ground-truth data further constrains external validation.

The five-class setup (rice, maize, root and tuber crops, other crops, and non-crop) and the use of class weighting helped prioritize the identification of staple crops relevant for flood impact assessment, but this likely came at the cost of increased false positives in some classes. While high recall ensures staple crops are identified, the

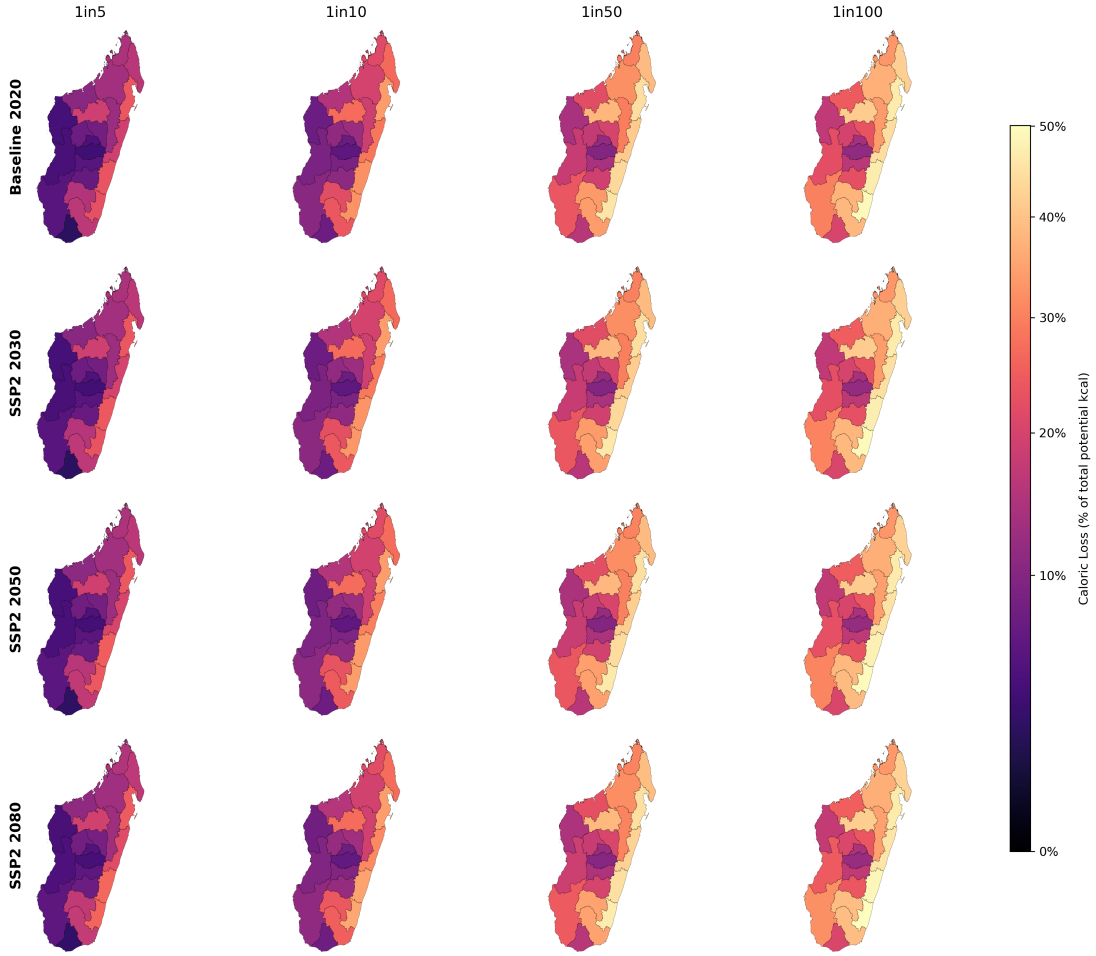

Figure 3. Comparison of caloric losses (in %) relative to potential availability under compound flooding, showing the 2020 baseline and future projections for 2030, 2050, and 2080 under SSP2.

lower precision for maize introduces a risk of overestimating exposed areas. Addressing this limitation, potentially through hierarchical classification architectures or by integrating street-level and drone imagery, is a primary focus for future iterations of this Work in Progress.

Comparison with national crop statistics and global datasets such as Dynamic World (Brown et al., 2022) and AFCD (Lou et al., 2025), reveals notable discrepancies. National statistics are primarily survey-based and subject to reporting biases, inconsistent crop definitions and temporal aggregation. In contrast, Dynamic World and AFCD are designed for global- or continent-wide predictions, which may not fully capture country-specific or local cropping patterns. The model-based classification, however, provides a spatially explicit and internally consistent representation of crop distribution for 2024 at the national scale. Despite some under- or overestimations in individual crop classes, the predicted areas generally fall within the plausible range indicated by these sources. Aggregation to administrative units further reduces the influence of local misclassifications, providing a robust basis for district-level flood and food loss assessments. These uncertainties propagate into downstream analyses of flood exposure and caloric loss, particularly for crops with lower classification performance.

Flood Exposure and Implications for Caloric Loss

The results show that rice is the most strongly affected crop in absolute terms, reflecting both its dominant role in national caloric production and its concentration in low-lying, flood-prone environments. Larger losses occur under high-return-period events (1-in-50 and 1-in-100) and become more pronounced under higher-emission pathways (e.g. SSP5-8.5), indicating that climate change may further intensify flood-related risks to staple crop production in Madagascar. At the same time, the district-level results reveal an important spatial contrast: the largest absolute caloric losses occur in the central production districts, particularly around Antananarivo, whereas some of the highest relative losses are found along the eastern coast. This distinction highlights that national food-system

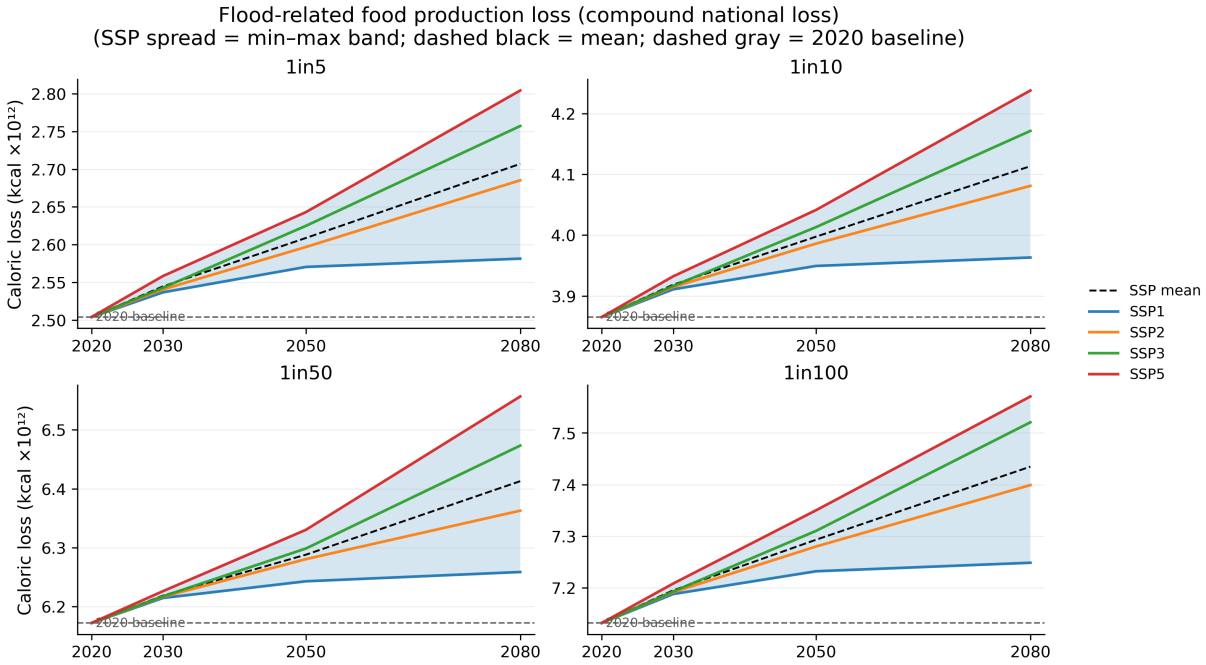

Figure 4. National caloric losses (in 10^{12} kcal) from compound flooding across return periods and SSPs relative to the 2020 baseline.

impacts are driven primarily by losses in the major production zones, while some highly exposed coastal districts are more severely affected in proportional terms.

The compound flood approach, which integrates fluvial, pluvial, and coastal hazards, highlights the interacting nature of flood drivers in Madagascar and the importance of accounting for these combined processes when assessing agricultural impacts. Neglecting this interaction would likely underestimate exposure and caloric loss, especially in cyclone-affected regions where multiple flood mechanisms can coincide.

At the same time, the analysis simplifies several important dynamics. First, the Fathom model provides maximum inundation depth but does not include flood duration or timing, both of which are critical for determining actual crop mortality and yield reduction. Second, additional uncertainties arise from the underlying climate scenarios, the flood hazard estimates, and the generalized caloric values per hectare, which do not capture the strong spatial and temporal heterogeneity of crop yields. Third, the present framework focuses on caloric production and therefore excludes livestock and non-food cash crops such as vanilla. Although these do not contribute directly to caloric availability, their loss can reduce household purchasing power and thereby represent an important indirect pathway to food insecurity.

Implications for Climate Adaptation and Food Security

The results indicate that both frequent and extreme compound flood events can substantially disrupt caloric availability in Madagascar. Under baseline conditions, the 1-in-10-year event results in losses of approximately 3.87×10^{12} kcal, equivalent to the annual minimum dietary energy requirements of about 5.1 million people. Under a more extreme future scenario, represented here by the 2080 SSP5–8.5 1-in-100-year event, projected losses rise to approximately 7.57×10^{12} kcal, corresponding to about 9.88 million people. Together, these results show that food-security risks are not limited to rare worst-case events, but may also emerge under more frequent floods that are more likely to recur within planning horizons relevant for adaptation and preparedness.

These projections should be interpreted with caution, as they assume static demographic and agricultural conditions. In reality, cropping regions may shift, certain crops may become less suitable under future climate conditions, and population growth will alter demand. The reported values should therefore be understood as baseline stress tests rather than literal forecasts. Even with this limitation, the framework provides useful insights not only for disaster management but also for longer-term climate-resilient agricultural planning, for example by helping identify regions where crop transitions, adaptation support, or targeted investment may become necessary.

Local agronomic interventions, such as early planting or early harvesting, can partially mitigate exposure to peak flood periods and reduce potential yield losses (Kruger, 2016). Nevertheless, even with such measures, staple

crops, especially rice, remain highly vulnerable under severe scenarios, underscoring the persistent risk to food security. Overall, the results illustrate the scale of climate-related flood risk and the potential for both recurrent and extreme events to disrupt caloric availability at the national level. More broadly, the findings suggest that farm-level adaptation must be complemented by wider policy measures, including climate adaptation, agricultural planning, and disaster risk reduction strategies, in order to reduce the likelihood and severity of such outcomes.

Implications for Disaster Management and Humanitarian Action

The transition from hazard-based monitoring to Impact-Based Forecasting represents a critical evolution for Decision Support Systems for crisis management. This study contributes to this shift by introducing a "caloric logic" that replaces abstract meteorological data with actionable information on human consequences. While traditional risk assessments often stop at exposure metrics (e.g., flooded hectares or number of affected people), this framework functions as a Socio-Technical Information Layer that quantifies the actual human cost of a hazard. By identifying districts where caloric losses are most acute, the system enables strategic resource allocation, informed, targeted preparedness, enabling humanitarian actors to prioritize regions based on nutritional deficits rather than raw flooded area (Sulser et al., 2021).

Current operational food security monitoring systems, such as USAID's Famine Early Warning Systems Network (FEWS NET, 2025), Integrated Food Security Phase Classification (IPC, 2025), and WFP's HungerMap (2026), rely primarily on indirect indicators, including rainfall anomalies, vegetation indices, market data, and expert assessments to infer potential impacts on food availability. While these approaches provide valuable early warning signals but often operate at broader livelihood-levels, they lack granularity to model how specific hazard footprints destroy agricultural yield at the field scale. This creates a 'decision gap' where humanitarian decision-makers recognize a regional threat but lack the tactical evidence to prioritize sub-districts for proactive Anticipatory Action (AA) or long-term resilience planning. To fill this gap, the framework developed in this study establishes a spatially-explicit linkage between hazard, crop exposure, and nutritional impact. By combining GeoAI-based crop type mapping with flood depth and crop-specific damage functions the model moves beyond proxy-based asssessments towards a physically grounded information system that provides granular, impact oriented evidence for trigger mechanisms for early action protocols. Finally, integrating these high-resolution outputs into Emergency Operations Centers (EOCs) moves the framework beyond simple situational awareness toward a dynamic Spatial Decision Support System (SDSS).

However, as a proof-of-concept, the current model has structural limitations that must be addressed before it can support operational food security decision-making. First, the model assesses caloric availability within district-level units, implicitly assuming that each unit functions in isolation. In reality, food systems operate as interconnected networks in which surplus regions can offset losses elsewhere. Second, the model does not account for international trade dynamics, despite Madagascar's food security being closely linked to global markets and import volatility. Third, crop availability in the field represents only one dimension of food security; actual impacts on populations are strongly mediated by physical accessibility, market functionality, and purchasing power.

A further priority for future work is to strengthen the temporal dimension of the framework. At present, yield loss is represented as a single annualized shock, whereas severe floods can damage infrastructure and degrade soils, resulting in recovery periods that extend over multiple growing seasons. Future iterations should therefore incorporate recovery functions to estimate multi-year caloric losses and link these losses with dynamic socio-economic vulnerability indicators (e.g., IPC phases) to assess whether shocks exceed local coping capacities.

CONCLUSION

This Work in Progress presents a spatially explicit, impact-based framework that combines crop type mapping with compound flooding scenarios to quantify agricultural vulnerability and potential caloric losses in Madagascar. By shifting the focus from physical exposure to nutritionally meaningful impact indicators, the framework identifies geographic hotspots where compound floods generate critical caloric losses. This approach provides the actionable evidence required for future Information Systems to move beyond situational awareness toward impact-based decision support, such as informing trigger designs for anticipatory action, pre-positioning food assistance, and guiding long-term preparedness under resource constraints.

However, to achieve full operational integration, a future research agenda must focus on three pillars:

- improve robustness in data-scarce settings by increasing classification precision for underrepresented crops through additional ground-truth data, improved quality control, and alternative modeling approaches

- incorporate crop seasonality by linking cropping calendars and growth stages to flood scenarios, enabling stage-sensitive loss estimates where suitable data are available
- strengthen validation with empirical evidence and co-design with practitioners to ensure the outputs can be integrated into operational impact-based forecasting and anticipatory action workflows

Finally, to support the transfer into practice, the workflow will be packaged as a reproducible, modular pipeline. This ensures that the methodological framework developed here can be adapted to other flood-prone regions, providing a scalable foundation for impact-based food security monitoring and climate-resilient crisis management.

ACKNOWLEDGEMENTS

This work was supported by the Klaus Tschira Stiftung (KTS). Computational and storage support was provided by Heidelberg University's Computing Center through the SDS@hd hot-data storage service, by the state of Baden-Württemberg through bwHPC and the bwForCluster Helix, and by the German Research Foundation (DFG) through grant INST 35/1597-1 FUGG.

REFERENCES

Adarsha, G., Veeresh, H., Rao, K., Gaddi, A. K., & Basavanneppa, M. (2019). Effect of foliar application of micronutrient mixture on growth and yield of maize (Zea mays L.) *Karnataka Journal of Agricultural Sciences*, *32*, 162–166.

Alves, A. F., Freitas, C. P. d. O. d., Zanon, A. J., Streck, N. A., Cardoso, P. d. S., & Tardetti, F. d. A. (2024). Water excess and its effect on cassava growth and yield. *Revista Ceres*, *71*, e71016. https://doi.org/10.1590/0034-737X2024710016

Brown, C. F., Brumby, S. P., Guzder-Williams, B., Birch, T., Hyde, S. B., Mazzariello, J., Czerwinski, W., Pasquarella, V. J., Haertel, R., Ilyushchenko, S., et al. (2022). Dynamic World, Near real-time global 10 m land use land cover mapping. *Scientific data*, *9*(1), 251. https://doi.org/10.1038/s41597-022-01307-4

Brown, C. F., Kazmierski, M. R., Pasquarella, V. J., Rucklidge, W. J., Samsikova, M., Zhang, C., Shelhamer, E., Lahera, E., Wiles, O., Ilyushchenko, S., Gorelick, N., Zhang, L. L., Alj, S., Schechter, E., Askay, S., Guinan, O., Moore, R., Boukouvalas, A., & Kohli, P. (2025). AlphaEarth Foundations: An embedding field model for accurate and efficient global mapping from sparse label data. https://arxiv.org/abs/2507.22291

Budhathoki, A., Tanaka, T., & Tachikawa, Y. (2024). Developing flood risk curves of agricultural economic damage under climate change in the Lower Chao Phraya River Basin, Thailand. *Journal of Flood Risk Management*, *17*(4), e13031. https://doi.org/10.1111/jfr3.13031

Butsko, C., Tricht, K. V., Tseng, G., Milli, G., Rolnick, D., Cartuyvels, R., Reshef, I. B., Szantoi, Z., & Kerner, H. (2025). Deploying Geospatial Foundation Models in the Real World: Lessons from WorldCereal. https://arxiv.org/abs/2508.00858

Cassidy, E. S., West, P. C., Gerber, J. S., & Foley, J. A. (2013). Redefining agricultural yields: From tonnes to people nourished per hectare. *Environmental research letters*, *8*(3), 034015. https://doi.org/10.1088/1748-9326/8/3/034015

Eisfelder, C., Boemke, B., Gessner, U., Sogno, P., Alemu, G., Hailu, R., Mesmer, C., & Huth, J. (2024). Cropland and crop type classification with Sentinel-1 and Sentinel-2 time series using Google Earth Engine for agricultural monitoring in Ethiopia. *Remote Sensing*, *16*(5), 866. https://doi.org/10.3390/rs16050866

European Commission, J. R. C. ((2025). Madagascar country assessment – agricultural production hotspots (asap) [Accessed: 2025-12-02]. https://agricultural-production-hotspots.ec.europa.eu/country.php?cntry=150

Famine Early Warning Systems Network. (2025). *FEWS NET: Famine early warning systems network*. Retrieved April 27, 2026, from https://fews.net/

Fathom. (2024). *Fathom global flood map*. Retrieved November 26, 2025, from https://www.fathom.global/product/global-flood-map/

Food and Agriculture Organization of the United Nations. (2025). *FAOSTAT: Crops and livestock products (QCL) database*. Retrieved December 2, 2025, from https://www.fao.org/faostat/en/#data/QCL

Foreign Agricultural Service. (2025). *Madagascar: Rice area, yield, and production data*. Retrieved December 2, 2025, from https://www.fas.usda.gov/data/production/MA

Global Yield Gap Atlas. (2025). *Global Yield Gap Atlas: Agricultural production and yield gap data*. Retrieved December 2, 2025, from https://www.yieldgap.org/

Gonzales-Valero, W. (2018). Hazards to food caloric availability and coverage per capita due to climate change in the Puno region, Peruvian Altiplano: Challenges in food security and sovereignty. *Food and Energy Security*, *7*(2), e00134. https://doi.org/10.1002/fes3.134

Integrated Food Security Phase Classification. (2025). *IPC: Integrated food security phase classification*. Retrieved April 27, 2026, from https://www.ipcinfo.org/

Khan, M. J. U., Durand, F., Afroosa, M., Coulet, P., Bertin, X., Mueller, V., Krien, Y., & Wainwright, C. (2025). Tropical cyclone induced compound flooding in Madagascar: a coupled modeling approach. *Natural Hazards*, *121*, 11013–11050. https://doi.org/10.1007/s11069-025-07209-z

Kruger, L. (2016). The timing of agricultural production in hazard-prone areas to prevent losses at peak-risk periods: A case of Malawi, Madagascar and Mozambique. *Jàmbá: Journal of Disaster Risk Studies*, *8*(2), Article 179, 1–9. https://doi.org/10.4102/jamba.v8i2.179

Lelong, C., & Herimandimby, H. (2022). Land use/land cover map of vavatenina region (madagascar) produced by object-based analysis of very high spatial resolution satellite images and geospatial reference data. *Data in Brief*, *44*, 108517. https://doi.org/10.1016/j.dib.2022.108517

Lou, Z., Peng, D., Shi, Z., Wang, H., Liu, K., Zhang, Y., Yan, X., Chen, Z., Ye, S., Yu, L., Hu, J., Lv, Y., Peng, H., Zhang, Y., & Zhang, B. (2025). An annual cropland extent dataset for Africa at 30 m spatial resolution from 2000 to 2022. *Earth System Science Data*, *17*, 3777–3796. https://doi.org/10.5194/essd-17-3777-2025

Molinari, D., Scorzini, A. R., Gallazzi, A., & Ballio, F. (2019). Agride-c, a conceptual model for the estimation of flood damage to crops: Development and implementation. *Natural Hazards and Earth System Sciences*, *19*, 2565–2582. https://doi.org/10.5194/nhess-19-2565-2019

Neubert, M., Höhnel, J., & Schinke, R. (2020). GIS-based Estimation of Flood Damage to Arable Crops, 183–194. https://doi.org/10.14627/537698017

Orynbaikyzy, A., Gessner, U., & Conrad, C. (2019). Crop type classification using a combination of optical and radar remote sensing data: A review. *International journal of remote sensing*, *40*(17), 6553–6595. https://doi.org/10.1080/01431161.2019.1569791

Pacetti, T., Caporali, E., & Rulli, M. C. (2017). Floods and food security: A method to estimate the effect of inundation on crops availability. *Advances in Water Resources*, *110*, 494–504. https://doi.org/10.1016/j.advwatres.2017.06.019

Park, S.-U., Lee, C.-J., Park, S.-C., Nam, K. J., Lee, K.-L., Kwak, S.-S., Kim, H. S., & Kim, Y.-H. (2022). Flooding Tolerance in Sweet Potato (Ipomoea batatas (L.) Lam) Is Mediated by Reactive Oxygen Species and Nitric Oxide. *Antioxidants*, *11*(5), 878. https://doi.org/10.3390/antiox11050878

Prokhorenkova, L., Gusev, G., Vorobev, A., Dorogush, A. V., & Gulin, A. (2018). CatBoost: Unbiased boosting with categorical features. *Advances in Neural Information Processing Systems*, *31*, 6638–6648. https://doi.org/10.48550/arXiv.1706.09516

Rigden, A. J., Golden, C., & Huybers, P. (2022). Retrospective predictions of rice and other crop production in Madagascar using soil moisture and an NDVI-based calendar from 2010–2017. *Remote Sensing*, *14*(5), 1223. https://doi.org/10.3390/rs14051223

Roberts, W., & Russo, V. (1991). Time of Flooding and Cultivar Affect Sweetpotato Yield. *HortScience*, *26*(12), 1473–1474. https://doi.org/10.21273/HORTSCI.26.12.1473

Sampson, C. C., Smith, A. M., Bates, P. D., Neal, J. C., Alfieri, L., & Freer, J. E. (2015). A high-resolution global flood hazard model. *Water resources research*, *51*(9), 7358–7381. https://doi.org/10.1002/2015WR016954

Sands, R. D. (2020). Global diets and demand for calories from crops. *2020 Annual Meeting of the Agricultural and Applied Economics Association*. https://doi.org/10.22004/ag.econ.304601

Stéphane, D., Laurence, D., Raffaele, G., Valérie, A., & Eloise, R. (2020). Land cover maps of Antananarivo (capital of Madagascar) produced by processing multisource satellite imagery and geospatial reference data. *Data in Brief*, *31*, 105952. https://doi.org/10.1016/j.dib.2020.105952

Sulser, T. B., Beach, R. H., Wiebe, K. D., Dunston, S., & Fukagawa, N. K. (2021). Disability-adjusted life years due to chronic and hidden hunger under food system evolution with climate change and adaptation to 2050. *The American Journal of Clinical Nutrition*, *114*(2), 550–563. https://doi.org/10.1093/ajcn/nqab101

Teluguntla, P., Thenkabail, P., Xiong, J., Gumma, M., Giri, C., Milesi, C., Ozdogan, M., Congalton, R., Tilton, J., Sankey, T., Massey, R., Phalke, A., & Yadav, K. (2015). Global Cropland Area Database (GCAD) derived from remote sensing in support of food security in the twenty-first century: Current achievements and future possibilities. In *Land resources: Monitoring, modelling, and mapping*. Taylor & Francis. https://pubs.usgs.gov/publication/70117684

Thompson, B., Cohen, M. J., & Meerman, J. (2012). World Food Insecurity and Malnutrition: Scope, Trends, Causes and Consequences. In B. Thompson & M. J. Cohen (Eds.), *The impact of climate change and bioenergy on nutrition* (pp. 21–41). Springer. https://doi.org/10.1007/978-94-007-0110-6_3

United Nations High Commissioner for Refugees & World Food Programme. (2024). *Emergency field operations pocketbook*. Retrieved April 14, 2026, from https://emergency.unhcr.org/sites/default/files/WFP%2C%20Emergency%20field%20operations%20pocketbook.pdf

Van Tricht, K., Degerickx, J., Gilliams, S., Zanaga, D., Battude, M., Grosu, A., Brombacher, J., Lesiv, M., Bayas, J. C. L., Karanam, S., et al. (2023). WorldCereal: a dynamic open-source system for global-scale, seasonal, and reproducible crop and irrigation mapping. *Earth System Science Data*, *15*(12), 5491–5515. https://doi.org/10.5194/essd-15-5491-2023

Wing, O. E., Bates, P. D., Quinn, N. D., Savage, J. T., Uhe, P. F., Cooper, A., Collings, T. P., Addor, N., Lord, N. S., Hatchard, S., et al. (2024). A 30 m global flood inundation model for any climate scenario. *Water Resources Research*, *60*(8), e2023WR036460. https://doi.org/10.1029/2023WR036460

World Bank Group. (2024). *Madagascar country climate and development report* [License: CC BY-NC-ND 3.0 IGO]. World Bank. http://hdl.handle.net/10986/42263

World Food Programme. (2025). All you need to know about the wfp food basket [Accessed 2026-04-14]. https://www.wfp.org/stories/wfp-food-basket

World Food Programme. (2026). *HungerMap LIVE*. Retrieved April 27, 2026, from https://hungermap.wfp.org/

WorldCereal. (2026). *WorldCereal classification module*. Retrieved April 27, 2026, from https://github.com/WorldCereal/worldcereal-classification